



## Highly conformal SiO<sub>2</sub>/Al<sub>2</sub>O<sub>3</sub> nanolaminate gas-diffusion barriers for large-area flexible electronics applications

**Author**  
Jin-Hwan Choi<sup>1</sup>, Young-Min Kim<sup>1</sup>, Young-Wook Park<sup>1</sup>, Tae-Hyun Park<sup>1</sup>, Jin-Wook Jeong<sup>1</sup>, Hyun-Ju Choi<sup>1</sup>, Eun-Ho Song<sup>1</sup>, Jin-Woo Lee<sup>2</sup>, Cheol-Ho Kim<sup>2</sup> and Byeong-Kwon Ju<sup>1</sup>

**Affiliations**  
<sup>1</sup>Display and Nanosystem Laboratory, College of Engineering, Korea University, 5-1 Anam-Dong, Seongbuk-Gu, Seoul 136-713, Korea  
<sup>2</sup>Display Materials Development Center, Cheil Industries Incorporated, 332-2 Gocheon-Dong, Uiwang-Si, Gyeonggi-Do 437-711, Korea  
<sup>3</sup>Author to whom any correspondence should be addressed

**E-mail**  
[bkju@korea.ac.kr](mailto:bkju@korea.ac.kr)

**Journal**  
[Nanotechnology](#)  [Create an alert](#)  [RSS this journal](#)

**Issue**  
[Volume 21, Number 47](#)

**Citation**  
Jin-Hwan Choi *et al* 2010 *Nanotechnology* **21** 475203  
doi: [10.1088/0957-4484/21/47/475203](https://doi.org/10.1088/0957-4484/21/47/475203)

[Article](#) [References](#)

 [Tag this article](#)  [Full text PDF \(1.10 MB\)](#)

### Users also read [What's this?](#)

1. Logic circuits based on individual semiconducting and metallic carbon-nanotube devices
2. Thermal activation and quantum field emission in a sketch-based oxide nanotransistor
3. Octreotide-modification enhances the delivery and targeting of doxorubicin-loaded liposomes to somatostatin receptors expressing tumor *in vitro* and *in vivo*

[More](#)

### Related review articles [What's this?](#)

1. Creating pure nanostructures from electron-beam-induced deposition using purification techniques: a technology perspective
2. Resists for sub-20-nm electron beam lithography with a focus on HSQ: state of the art
3. Recent developments in inorganically filled carbon

Quick search

Title/Abstract ▾

All Dates ▾

All journals  This journal only

## Table of contents

[Create an alert](#)  [RSS this journal](#) 

### Nanotechnology Volume 21

Number 47, 26 November 2010    [« previous](#)    [next »](#)

## Journal links

[Journal home](#)

[Scope](#)

[Editorial board](#)

[Abstracted in](#)

[Author benefits](#)

## Highly conformal SiO<sub>2</sub>/Al<sub>2</sub>O<sub>3</sub> nanolaminate gas-diffusion barriers for large-area flexible electronics applications

This article has been downloaded from IOPscience. Please scroll down to see the full text article.

2010 Nanotechnology 21 475203

(<http://iopscience.iop.org/0957-4484/21/47/475203>)

View [the table of contents for this issue](#), or go to the [journal homepage](#) for more

Download details:

IP Address: 144.92.202.36

The article was downloaded on 30/10/2010 at 18:51

Please note that [terms and conditions apply](#).

# Highly conformal SiO<sub>2</sub>/Al<sub>2</sub>O<sub>3</sub> nanolaminate gas-diffusion barriers for large-area flexible electronics applications

Jin-Hwan Choi<sup>1</sup>, Young-Min Kim<sup>1</sup>, Young-Wook Park<sup>1</sup>,  
Tae-Hyun Park<sup>1</sup>, Jin-Wook Jeong<sup>1</sup>, Hyun-Ju Choi<sup>1</sup>, Eun-Ho Song<sup>1</sup>,  
Jin-Woo Lee<sup>2</sup>, Cheol-Ho Kim<sup>2</sup> and Byeong-Kwon Ju<sup>1,3</sup>

<sup>1</sup> Display and Nanosystem Laboratory, College of Engineering, Korea University, 5-1 Anam-Dong, Seongbuk-Gu, Seoul 136-713, Korea

<sup>2</sup> Display Materials Development Center, Cheil Industries Incorporated, 332-2 Gocheon-Dong, Uiwang-Si, Gyeonggi-Do 437-711, Korea

E-mail: [bkju@korea.ac.kr](mailto:bkju@korea.ac.kr)

Received 16 August 2010, in final form 28 September 2010

Published 29 October 2010

Online at [stacks.iop.org/Nano/21/475203](http://stacks.iop.org/Nano/21/475203)

## Abstract

The present study demonstrates a flexible gas-diffusion barrier film, containing an SiO<sub>2</sub>/Al<sub>2</sub>O<sub>3</sub> nanolaminate on a plastic substrate. Highly uniform and conformal coatings can be made by alternating the exposure of a flexible polyethersulfone surface to vapors of SiO<sub>2</sub> and Al<sub>2</sub>O<sub>3</sub>, at nanoscale thickness cycles via RF-magnetron sputtering deposition. The calcium degradation test indicates that 24 cycles of a 10/10 nm inorganic bilayer, top-coated by UV-cured resin, greatly enhance the barrier performance, with a permeation rate of  $3.79 \times 10^{-5} \text{ g m}^{-2} \text{ day}^{-1}$  based on the change in the ohmic behavior of the calcium sensor at 20 °C and 50% relative humidity. Also, the permeation rate for 30 cycles of an 8/8 nm inorganic bilayer coated with UV resin was beyond the limited measurable range of the Ca test at 60 °C and 95% relative humidity. It has been found that such laminate films can effectively suppress the void defects of a single inorganic layer, and are significantly less sensitive against moisture permeation. This nanostructure, fabricated by an RF-sputtering process at room temperature, is verified as being useful for highly water-sensitive organic electronics fabricated on plastic substrates.

(Some figures in this article are in colour only in the electronic version)

## 1. Introduction

The growing interest in thin film flexible organic electronics has led to an increasing number of applications of organic light-emitting diodes (OLEDs), organic solar cells and organic thin film transistors (OTFTs) [1–4]. It is widely known that organic devices are highly susceptible to the permeation of water and oxygen [5]. The permeation region  $<10^{-5} \text{ g m}^{-2} \text{ day}^{-1}$  is of particular commercial interest due to the organic display lifetime of  $>10\,000 \text{ h}$  [6–8]. Alumina- and silica-based materials are the current choices for moisture-diffusion barrier applications, and are usually applied to organic-based electrical devices [7–10]. These materials could

be deposited by various physical and chemical techniques, such as evaporation, oxidation, chemical vapor deposition, plasma polymerization and nanocompositions [7–14].

However, inorganic materials are notorious for cracking, and for having pinhole defects in the layer surface [8, 9, 15–17]. The reported water vapor transmission rate (WVTRs) values, for such materials, are about  $10^{-1} \text{ g m}^{-2} \text{ day}^{-1}$  [18], and so highly impermeable protection technologies are required. For the fabrication of ultralow gas-diffusion barrier films, Weaver *et al* [6] proposed organic/inorganic multi-barrier stacks. Also, Carcia *et al* [8, 9] showed that films fabricated by atomic-layer deposition have higher barrier efficiencies. However, thin film barriers with ultralow permeation rates should have high productivity and use a low-cost fabrication process.

<sup>3</sup> Author to whom any correspondence should be addressed.

This paper proposes the use of inorganic nanolaminate gas-diffusion barrier films prepared by RF sputtering at room temperatures. Sputtering deposition using RF guns has the advantage of being a simplified process for handling industrial-scale coatings as well as allowing simultaneous deposition of various kinds of materials, through the use of more than two RF guns. Also, it offers a number of remarkable industrial capabilities in addition to film uniformity and easy composition of the films. A nanolaminate barrier is a film composed of deposited alternating layers of SiO<sub>2</sub> and Al<sub>2</sub>O<sub>3</sub> which provide extremely extended gas-diffusion pathways, leading to ultralow WVTRs.

## 2. Experimental details

Thin gas barriers are deposited on polyethersulfone (PES, 150  $\mu\text{m}$  thickness, Cheil Industries Inc., Korea) substrates using the dual-gun RF-magnetron sputtering system. The deposition order is considered based on the surface energies of the material itself. For optimized barrier performance, the above method is an effective way to deposit the outer Al<sub>2</sub>O<sub>3</sub> layer because of the water absorption property of the SiO<sub>2</sub> hydrophilic surface [19–21]. The top Al<sub>2</sub>O<sub>3</sub> and the intermediate SiO<sub>2</sub> layers are placed, based on their surface energies of 40.2 and  $>73.12 \text{ mN m}^{-1}$ , calculated by surface contact angle measurements based on Owens' equation [22], as shown in figure 1(a). Figure 1(b) shows the surface contact images of a DI water droplet on the barrier-coated PES. The contact angle values are given by software measurements of 73.95° for the DI water and 40.12° for the formamide on Al<sub>2</sub>O<sub>3</sub> (both of the contact angles on the SiO<sub>2</sub> were  $<5^\circ$ ).

This research has targeted SiO<sub>2</sub>/Al<sub>2</sub>O<sub>3</sub> (SA) bilayers because both are utilized as gas-diffusion barriers on plastic substrates. The base pressure of the RF-sputtering process was 2 mTorr in Ar flow conditions. The RF powers of 250 and 150 W for SiO<sub>2</sub> and Al<sub>2</sub>O<sub>3</sub> deposition have been utilized at 5 sccm with a deposition rate of 7.32 nm min<sup>-1</sup> for the SiO<sub>2</sub> layer along with a deposition rate of 2.00 nm min<sup>-1</sup> for the Al<sub>2</sub>O<sub>3</sub> layer at room temperature.

The quantitative analysis of WVTRs of the order of 10<sup>-6</sup> g m<sup>-2</sup> day<sup>-1</sup> for water is very challenging because the measurable range of the commonly used system is limited to 10<sup>-3</sup> g m<sup>-2</sup> day<sup>-1</sup> [23]. Therefore, the gas barrier performances of nanolaminated films are characterized using the calcium degradation test by monitoring the change in ohmic behavior of the thin film of Ca [24, 25]. Ca is sensitive to water and oxygen. On the assumption that WVTRs dominate in the reaction between Ca and vapor, water permeation rates can be said to be the main factor for the degradation of organic devices. As shown in figure 1(c), Ag electrodes (250 nm thickness) and Ca pads (100 nm thickness) are thermally deposited on a highly impermeable glass substrate through shadow masks. The Ca sensor has an active area of 4 cm<sup>2</sup> and is encapsulated by the films in a glove-box system. The permeation rates through the UV epoxy as a sealing material should be less than 10<sup>-6</sup> g m<sup>-2</sup> day<sup>-1</sup>. Previously [25], we have measured the permeation rate of a glass lid sealed by epoxy with a width of about 3 mm and it satisfied the

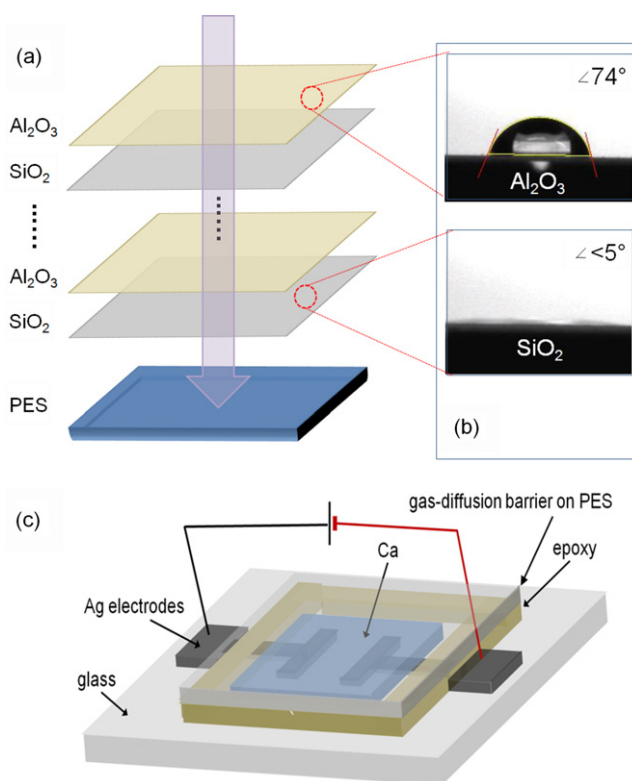


**Figure 1.** (a) Schematic diagram of inorganic bi-deposited nanolamination and (b) DI water droplet contact images of the surfaces of single inorganic layers on PES. (c) The structure of the Ca test.

permeation rates of  $<10^{-6} \text{ g m}^{-2} \text{ day}^{-1}$ . Then, sensors are transferred to a controlled environmental chamber at 20 °C and 50% relative humidity (RH), and 60 °C and 95% RH. After encapsulation of the Ca film, the test sample is exposed to air and the increase in resistance of the calcium film is simultaneously measured with time, due to the oxidation of Ca by water permeation.

## 3. Results and discussion

### 3.1. Analysis of moisture barrier with nanoscale resolution

Previous reports have identified defects such as pinholes and grain boundaries as primary diffusion paths in the inorganic layers [15–17, 26]. For this reason, a series resistance model for a multilayered system and inorganic laminate films has been proposed in an attempt to increase the lag-time of the moisture permeation process [26, 27]. In a previous review, laminate theory has predicted a total permeability of  $1/P_T = \sum 1/P_L$ , where  $P_L$  is the permeability of the individual layer [26]. The permeability is reduced substantially if the individual layers in the multilayer act to cover the defects in the adjacent layers.

Figure 2(a) shows cross-sectional high resolution transmission electron microscopy (HRTEM, Tecnai 20) images of cleaved and etched 10/10 nm SiO<sub>2</sub>/Al<sub>2</sub>O<sub>3</sub> (SA) nanolaminate bilayers prepared by a focused ion beam (FIB) technique, on an Si wafer, in order to analyze the barrier films at



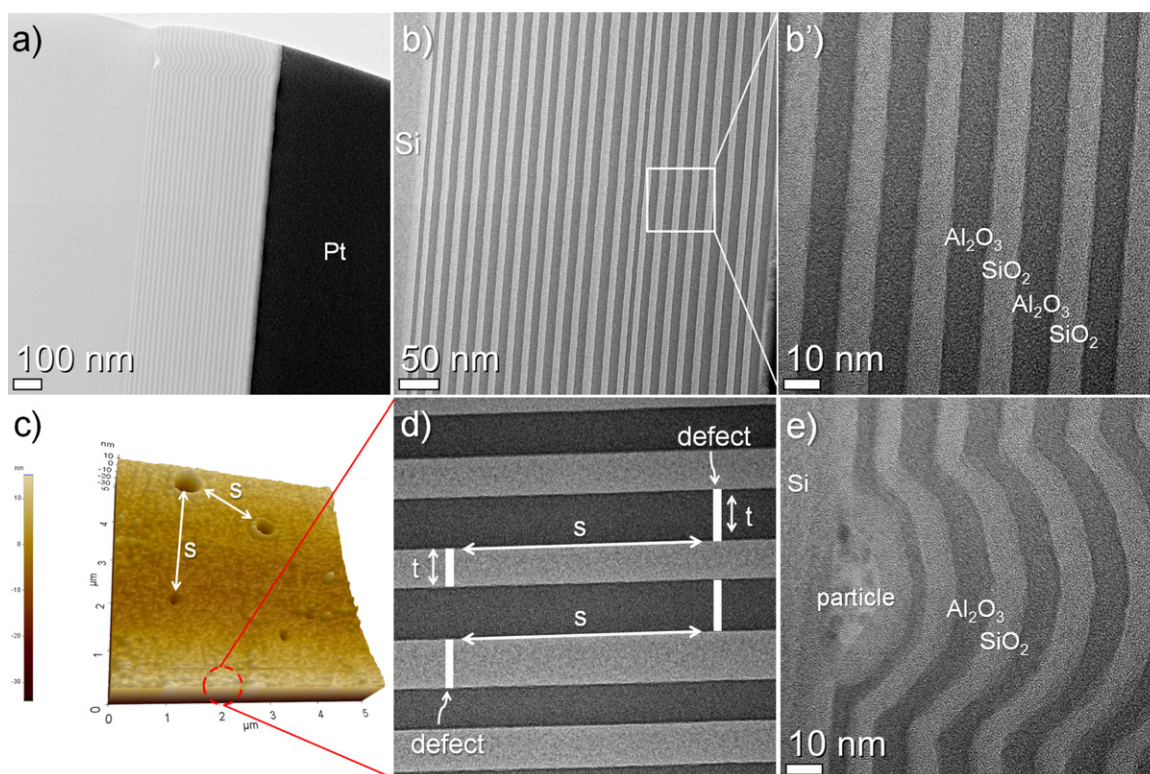


**Figure 2.** (a) Cross-sectional HRTEM images of 24 cycles of 10/10 nm SA films on Si wafer prepared by the FIB process with (b) magnified view and (c) AFM image of  $\text{Al}_2\text{O}_3$  surface deposited on PES substrate. Micrometer scale defects are shown with spacing  $s$  between them and (d) schematic illustration of the diffusion length of the barrier layer. (e) The small impurity particles originated from the substrate were not inherent to the continuously sputtered SA films.

the nanometer scale. In the magnified view, shown in figure 2(b), the subsequent 10 nm amorphous SA are sufficient to demonstrate that the formation of diffusion paths due to water molecule permeation along the nanosized grain boundary can be effectively suppressed. The TEM images of the sputtered  $\text{SiO}_2$  and  $\text{Al}_2\text{O}_3$  films show excellent conformity. The thickness is linear in the number of pairs of layers (cycles). In this case, defects in the  $\text{SiO}_2$  and  $\text{Al}_2\text{O}_3$  are so far apart that the gas-diffusion vector is almost parallel to the plane of each layer, extending the diffusion path between the  $\text{SiO}_2$  and  $\text{Al}_2\text{O}_3$  layers. In figure 2(c), the atomic force microscope (AFM, XE-100) image shows the size (about 0.1–0.5  $\mu\text{m}$ ) of defects and the spacing diameter ( $>1 \mu\text{m}$ ) between them. For a film of physical thickness  $t$  and defect spacing  $s$ , when  $t \ll s$ , the diffusion path ( $l$ ) is about

$$l = t_1 + s_1 + \dots + t_n + s_n \approx ns \quad (1)$$

as shown schematically in figure 2(d).

Also, many researchers believe that small impurities such as dust particles on the polymer surface induce the defects during the barrier deposition process and can affect the film performances. However, the present case shows that the defects in the sealing layer do not originate from the substrate as a result of particle or surface roughness. These defects were not inherent to the continuously sputtered SA films and so, as shown in figure 2(e), sputtered inorganic laminate films successfully cover the particles on the polymer surface.

### 3.2. Moisture permeation rates

To understand the effect of the nanolaminate films, WVTRs were measured for the single  $\text{SiO}_2$  and  $\text{Al}_2\text{O}_3$  films, previously. The gas barrier performances of the films are characterized using the calcium degradation test by monitoring the change in ohmic behavior of the thin film of Ca [24, 25]. Compared to the WVTR ( $1.38 \text{ g m}^{-2} \text{ day}^{-1}$ ) of bare PES, the WVTRs of the single barrier layer (480 nm thickness) of  $\text{SiO}_2$  and  $\text{Al}_2\text{O}_3$  on PES are  $1.81 \times 10^{-1}$ , and  $3.02 \times 10^{-1} \text{ g m}^{-2} \text{ day}^{-1}$  at 20 °C and 50% RH, respectively. Also, the WVTR of a composite film of  $\text{SiO}_2$  and  $\text{Al}_2\text{O}_3$  by simultaneous deposition using RF sputtering is  $3.45 \times 10^{-1} \text{ g m}^{-2} \text{ day}^{-1}$ .

To evaluate the performance of increasing the number of cycles of SA bilayer film concretely, four types of laminate films are fabricated on PES where each of the samples has the same total thickness. Figure 3(a) shows the curves of Ca conductance over time as a function of the cycles of SA bilayers. The Ca test indicates that 4 cycles of 60/60, 8 cycles of 30/30, 12 cycles of 20/20 nm and 24 cycles of 10/10 nm SA barrier films yield WVTRs of  $1.04 \times 10^{-1}$ ,  $3.11 \times 10^{-2}$ ,  $9.45 \times 10^{-3}$  and  $3.5 \times 10^{-4} \text{ g m}^{-2} \text{ day}^{-1}$ , respectively. Depending on the applicable mechanism of moisture diffusion, the laminated SA bilayers provide significant improvement. Also, this behavior is known to be consistent with the gas permeation through the crack and pinhole defects in the inorganic films.

In our SA nanolaminate barriers, some approaches preventing  $\text{Al}_2\text{O}_3$  corrosion are expected. Dameron *et al* have

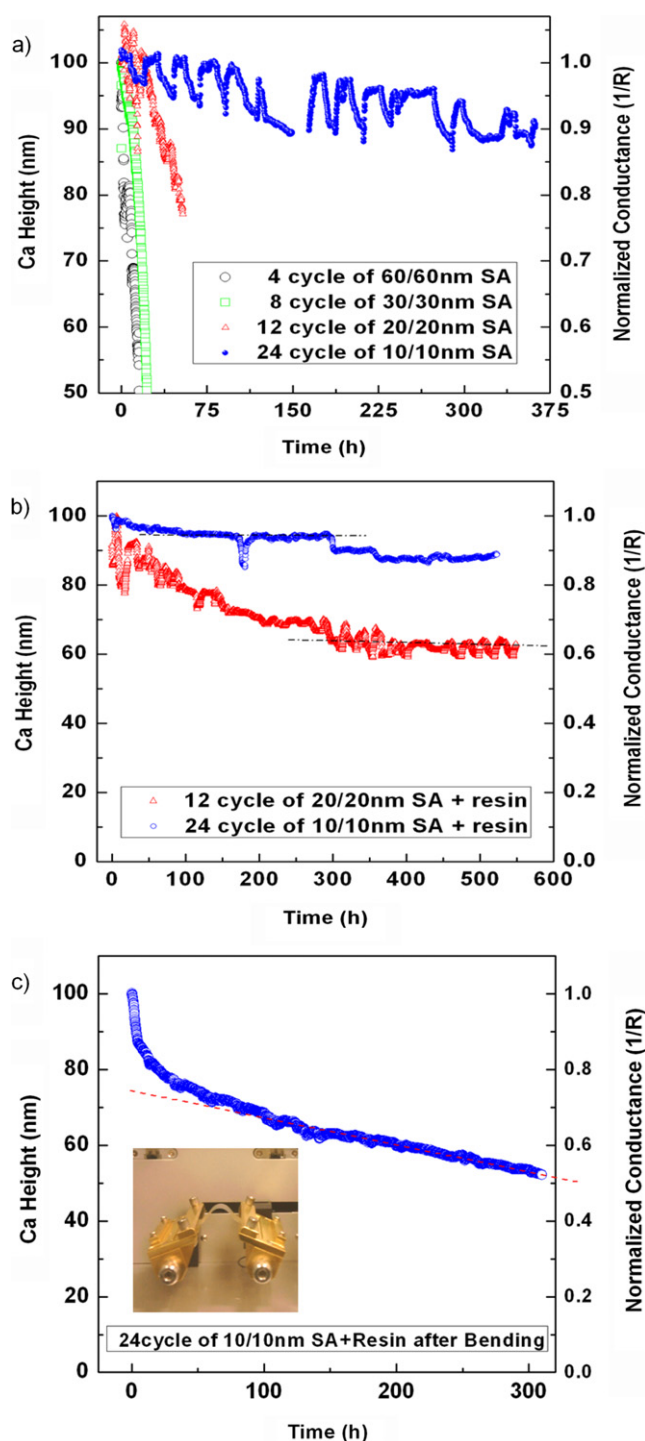


**Figure 3.** (a) Electrical curves induced by Ca degradation due to moisture permeation. These barrier films on PES substrates have the same barrier thickness of 480 nm. (b) Permeation curves of impermeable barrier layer comprising 12 cycles of a 20/20 nm SA layer and 24 cycles of a 10/10 nm SA layer coated with UV-cured resin. (c) Ca degradation curve of the film after 1000 cycles of a bending process. Inset image shows the bending tester and the flexible film with the moisture barrier.

reported that corrosion of  $\text{Al}_2\text{O}_3$ , due to moisture permeation, deteriorates the diffusion barrier functionality [8, 17]. To prevent moisture-induced corrosion of the top  $\text{Al}_2\text{O}_3$  film, the

UV-cured resin ( $1 \mu\text{m}$  thickness) is coated onto the inorganic barrier surface by a dropping and UV-curing process. Also, the organic buffer is used as a smoothing, strengthening, flexible and defect decoupling layer. This film, composed of a UV resin, inside the inorganic nanolaminate bilayer, showed ultralow permeation characteristics. As shown in figure 3(b), notably, 24 cycles of 10/10 nm SA laminate with the top-coated UV-cured resin, ultralow permeation rate  $3.79 \times 10^{-5} \text{ g m}^{-2} \text{ day}^{-1}$  at  $20^\circ\text{C}$  and 50% RH for water have been measured (the permeation rate of 12 cycles of SA films with resin is  $1.87 \times 10^{-4} \text{ g m}^{-2} \text{ day}^{-1}$ ).

In addition to enhanced barrier performance through inorganic lamination, its mechanical flexibility has also been tested. WVTRs of 24 cycles of 10/10 nm SA laminate with UV-cured resin coating was measured after 1000 cycles of the bending process (Z-100 Bending Tester, refer to the inset of figure 3(c)). The bending radius of the film was 10 mm. Figure 3(c) shows the Ca degradation curve of the film, which indicates that the permeation rate is  $1.64 \times 10^{-3} \text{ g m}^{-2} \text{ day}^{-1}$ . This was a worse barrier characteristic than for the films before bending. However, methods such as increasing the alternating cycles, insertion of elastic materials as an interlayer [28, 29] and decreasing the thickness of the inorganic layer can be solutions when applying bending stress with an extremely low radius curvature. For this reason this work remains to be performed for immediate commercial applications. The slopes of the Ca conductance versus the elapsed time curves are linear and indicate the average permeation rates. Water vapor residues on the plastic film can permeate the Ca layer and react with it. This can account for the degrading region in the initial stages of measurement. The electrical measurement system used can also be affected by current leakage and fluctuation. As a result, accurate reading of permeation rates is limited by the region of electrical variation. Measurement over longer time durations can help improve the accuracy of the results.

For evaluation of extremely low moisture permeation, 30 cycles of 8/8 nm SA laminate film with UV resin were measured at  $20^\circ\text{C}$  with 50% RH, and at  $60^\circ\text{C}$  with 95% RH. Figure 4 shows the conductance curves of Ca in relation to elapsed time. Figure 4(a) shows a magnified curve for the film and the dashed line indicates a permeation rate of  $0 \text{ g m}^{-2} \text{ day}^{-1}$ . In figure 4(b), the curves of the film at  $60^\circ\text{C}$  and 95% RH show no degradation in performance compared to  $0 \text{ g m}^{-2} \text{ day}^{-1}$ . The reason for these results is because the films have permeation rates beyond the limit of measurable range of the Ca test ( $10^{-6} \text{ g m}^{-2} \text{ day}^{-1}$ ). While changing the environmental conditions, an electric wire was added, resulting in a slight increase in resistance of the test sample as shown in figure 4(c) (not affected by water permeation).

The question also arises as to whether the number of cycles and barrier thickness play an important role. Therefore, additional experiments on the inorganic laminate bilayer have been performed by reducing the layer thickness in order to determine its effectiveness on the barrier performance. From the results it is concluded that the layer thickness, when it is less than the critical thickness of  $<5 \text{ nm}$  deposited by RF sputtering, could be easily transited by the water molecules. This may be inferred from previous experiments in which a



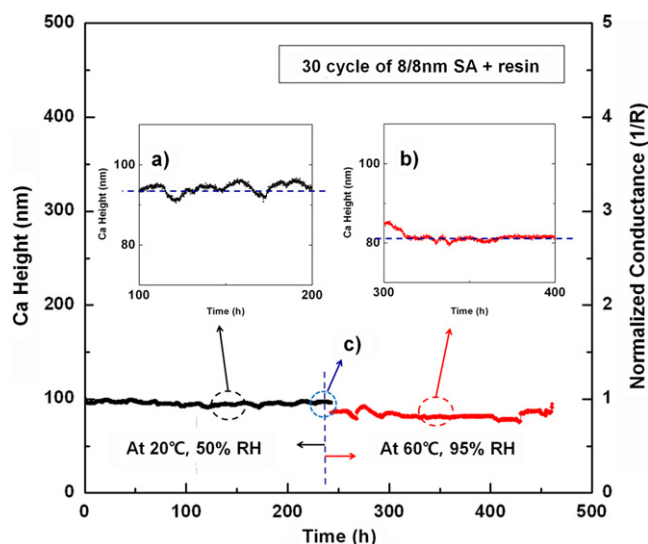


**Figure 4.** Ca degradation curve of 30 cycles of an 8/8 nm SA with UV-cured resin at 20 °C with 50% RH, and 60 °C with 95% RH, respectively. Both magnified views of curves at (a) 20 °C and 50% RH, and at (b) 60 °C and 95% RH show the permeation rates are beyond the limit of measurable range of the Ca test and dashed lines indicate a permeation rate of  $0 \text{ g m}^{-2} \text{ day}^{-1}$ . (c) Electrical wire added for the measurement of different environmental conditions increased the resistance of the Ca-test cell.

single layer of  $\text{Al}_2\text{O}_3$ , grown by RF sputtering, with  $<5 \text{ nm}$  thickness, has been found to have no independent role as the dielectric layer.

### 3.3. Light transmittance values of the films and Ca sensor

Figure 5(a) represents the transmittance spectrum of the films in the visible region, characterized by a UV-vis spectrometer (Agilent 8453). We have measured two samples (films). One is 24 cycles of 10/10 nm SA nanolaminated barrier on PES (reference), while the other is just bare PES (before the barrier coating process). The two films showed almost the same transmittance values. Both are over 82% in the visible wavelength. The total light transmission rates of these films are generally above 82%, reaching 89% in the best cases. As can be seen in figure 5(b), the films are not blurred and can be applicable to optical devices. Figure 5(c) shows the optical images of Ca cells encapsulated by PES, coated with 4 cycles of 60/60 nm thickness of SA and 24 cycles of 10/10 nm SA, before and after  $\sim 200 \text{ h}$ , where the transparent  $\text{Ca}(\text{OH})_2$  is produced as an insulator by the reaction between Ca and  $2\text{H}_2\text{O}$ . Also, we can see a large difference in the quantity of oxidation between the two samples after 200 h.

## 4. Conclusion

In conclusion, this paper has presented  $\text{SiO}_2$  and  $\text{Al}_2\text{O}_3$  nanolaminate films on PES, deposited by Ar-plasma dual-sputtering processes at room temperature, and WVTRs through the laminated films have been determined using the electrical Ca test. This approach could be effective for the facile and

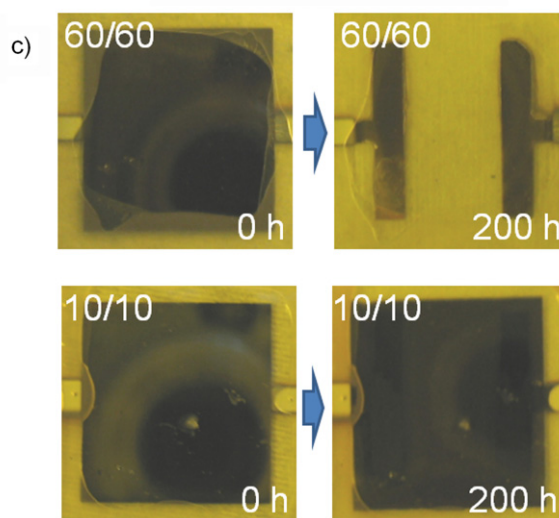
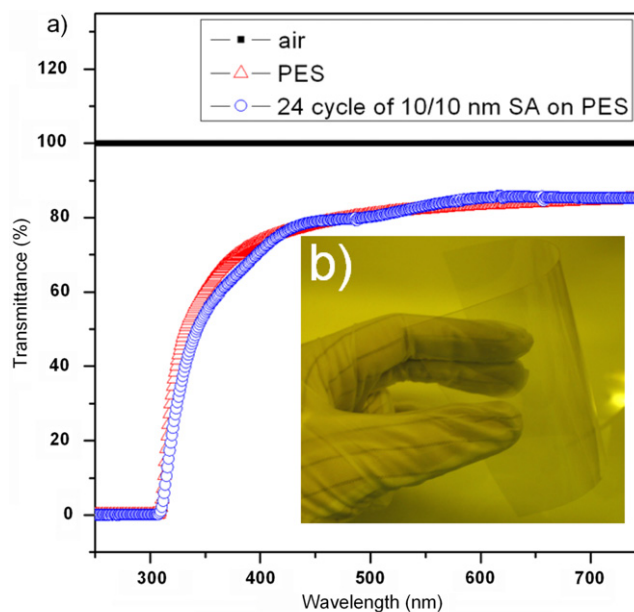


**Figure 5.** (a) The light transmission curves of bare PES and laminated films on PES, and (b) photographs of a flexible gas-diffusion barrier film. (c) Photo images of optical changes in the barrier-coated Ca cells over time. Ca-test cell has been encapsulated by 4 cycles of 60/60 nm SA and 24 cycles of 10/10 nm SA barrier layers.

rapid fabrication method of the gas barrier film, and could yield permeation rates of  $3.79 \times 10^{-5} \text{ g m}^{-2} \text{ day}^{-1}$ , in an environment of 20 °C and 50% RH, and beyond the limit of the measurable range ( $10^{-6} \text{ g m}^{-2} \text{ day}^{-1}$ ) of the Ca-test even at 60 °C and 95% RH. The nanolaminate architecture has been demonstrated to effectively suppress void defect formation, as a result of this method, as there is an increase in the bilayer steps. Because of decreased permeation rates and extreme conformity, the alternating layer deposition will be useful for many applications; hence, this simple and fast method can be suitable for use in such cases as large area, mass coating processes in many applications, due to the reliable gas barrier performance with high light transmission.



## Acknowledgments

This work was supported by the RFID R&D program of MKE/KEIT. [10035225, Development of core technology for high performance AMOLED on plastic], and supported by a Grant-in-Aid (10030041-2009-12) under the Next-Generation New Technology Development Programs from the Ministry of Knowledge Economy of the Korean government. And this research was supported by the Basic Science Research Program through the National Research Foundation of Korea (NRF) funded by the Ministry of Education, Science and Technology (CAFDC-20100009869).

## References

- [1] Chwang A B et al 2003 *Appl. Phys. Lett.* **83** 413–5
- [2] Wu Z, Wang L, Chang C and Qiu Y 2005 *J. Phys. D: Appl. Phys.* **38** 981–4
- [3] Lee T, Chung Y, Kwon O and Park J 2007 *Adv. Funct. Mater.* **17** 390–6
- [4] Hauch J A, Schilinsky P, Choulis S A, Rajoelson S and Brabec C 2008 *Appl. Phys. Lett.* **93** 103306
- [5] Schaer M, Nuesch F, Berner D, Leo W and Zuppiroli L 2001 *Adv. Funct. Mater.* **11** 116–21
- [6] Weaver M S et al 2008 *Appl. Phys. Lett.* **81** 2929–31
- [7] Yun S J, Ko Y and Lim J W 2004 *Appl. Phys. Lett.* **85** 4896–8
- [8] Dameron A A, Davidson S D, Burton B B, Carcia P F, Mclean R S and George S M 2008 *J. Phys. Chem. C* **112** 4573–80
- [9] Carcia P F, Mclean R S, Reilly M H, Groner M D and George S M 2006 *Appl. Phys. Lett.* **89** 031915
- [10] Chen T N, Wu D S, Wu C C, Chiang C C and Chen Y P 2006 *J. Electrochem. Soc.* **153** F244–8
- [11] Hausmann D, Becker J, Wang S and Gordon R G 2002 *Science* **298** 402–6
- [12] Zambov L, Weidner K, Shamamian V, Camilletti R, Pernisz U, Loboda M, Cerny G, Gidley D, Peng H and Vallery R 2006 *J. Vac. Sci. Technol. A* **24** 1706–13
- [13] Sun H Y, Lau K M, Lau K C, Chan M Y, Fung M K, Lee C S and Lee S T 2006 *Appl. Phys. Lett.* **88** 223503
- [14] Ebina T and Mizukami F 2007 *Adv. Mater.* **19** 2450–3
- [15] Lim S F, Ke L, Wang W and Chua S J 2001 *Appl. Phys. Lett.* **78** 2116
- [16] Chen T, Wu D, Wu C, Chiang C, Chen Y and Horng R 2007 *Plasma Process. Polym.* **4** 180–5
- [17] Kim N, Potscavage W J, Domercq B, Kippelen B and Graham S 2009 *Appl. Phys. Lett.* **94** 163308
- [18] Choi J, Kim Y, Park Y, Park T, Dong K and Ju B 2009 *Nanotechnology* **20** 135303
- [19] Parker A R and Lawrence C R 2001 *Nature* **414** 33–4
- [20] Zhai L, Berg M C, Cebeci F C, Kim Y and Milwid J M 2006 *Nano Lett.* **6** 1213–7
- [21] Choi J H, Kim Y M, Park Y W, Park T H, Dong K Y and Ju B K 2009 *Langmuir* **25** 7156–60
- [22] Owens D K and Wendt R C 1969 *J. Appl. Polym. Sci.* **13** 1741–7
- [23] Dunkel R, Bujas R, Klein A and Horndt V 2005 *Proc. IEEE* **93** 1478–82
- [24] Paetzold R, Winnacker A, Henseler D, Cesari V and Heuser K 2003 *Rev. Sci. Instrum.* **74** 5147–50
- [25] Choi J H, Kim Y M, Park Y W, Huh J W, Kim I S, Hwang H N and Ju B K 2007 *Rev. Sci. Instrum.* **78** 064701
- [26] Graff G L, Williford R E and Burrows P E 2004 *J. Appl. Phys.* **96** 1840–9
- [27] Meyer J, Gorrn P, Bertram F, Hamwi S, Winkler T, Johannes H, Weimann T, Hinze P, Riedl T and Kowalsky W 2009 *Adv. Mater.* **21** 1–5
- [28] Jeong J, Kim H and Yi M 2008 *Appl. Phys. Lett.* **93** 033301
- [29] Hanada T, Negishi T, Shiroishi I and Shiro T 2010 *Thin Solid Films* **518** 3089–92